Available online at www.sciencedirect.com

ScienceDirect

Procedia Manufacturing 36 (2019) 101–111

Procedia MANUFACTURING

www.elsevier.com/locate/procedia

17th Nordic Laser Material Processing Conference (NOLAMP17), 27 – 29 August 2019

Porosity and solidification cracking in welded 45 mm thick steel by fiber laser-MAG process

Ivan Bunaziv[a,*], Jan Frostevarg[b], Xiaobo Ren[a], Alexander F.H. Kaplan[b], Odd M. Akselsen[a]

[a] *SINTEF Industry, P.O. Box 4760 Torgarden, NO-7465 Trondheim, Norway*
[b] *Luleå University of Technology, Department of Engineering Sciences and Mathematics, SE-97187 Luleå, Sweden*

Abstract

Porosity and solidification cracking in joining of thick sections are very common issues in deep penetration keyhole laser-arc hybrid welding (LAHW). In the present work, 45 mm thick high strength steel was joined by a double-sided technique. With combined use of fast welding speeds and larger air gap between plates, higher amount of porosity was found because of the dynamic behavior of the keyhole walls. Solidification cracking formed at the centerline in the bottom of the weld due to high-depth-to-width geometrical ratio. Numerical simulations have been performed and showed very high cooling rate and stresses occurred in the root of the deep welds, which corresponds with higher cracking tendency.

Peer-review under responsibility of the scientific committee of the 17th Nordic Laser Material Processing Conference.

Keywords: Laser welding; hybrid welding; solidification cracking; porosity; thick steel; mechanical properties

1. Introduction

Deep penetration laser-arc hybrid welding (LAHW) is a promising process for joining thick (> 10 mm) steel plates in one-pass technique. Due to high penetration depth provided by keyhole mode, it can offer substantial increase of productivity. However, this process is susceptible to solidification cracking and porosity.

Porosity problems can cause substantial deterioration in mechanical properties of the welds. It is generally accepted that the keyhole (the cavity filled with metal vapour) collapse is the main factor for porosity occurrence due to its unstable dynamics causing trapped gas rounded cavities (or bubbles) which cannot escape from the molten metal pool

* Corresponding author. Tel.: +47 45795269.
E-mail address: ivan.bunaziv@sintef.no

2351-9789
Peer-review under responsibility of the scientific committee of the 17th Nordic Laser Material Processing Conference.
10.1016/j.promfg.2019.08.015

during solidification. In deep and narrow welds (high depth-to-width-ratio), porosity tends to be higher since gas pores should have longer time for escape compared to shallow and wide welds due to longer transport distance. Porosity can also occur from trapped shielding gas during processing. However, these pores are much less frequent and appear in the upper part of the weld.

There are numerous studies on porosity formation in aluminum alloys, due to its high susceptibility to this defect. For example, according to Katayama et al. [1, 2] porosity formation is caused by unfavorable melt flows confirmed by X-ray filmography. An increase of the current in LAHW suppresses bubble formation due to weld pool depression, wider weld pool and favorable melt flows. However, it is most likely to work only for thin sheet case. Recent studies by Miyagi et al. [3] using X-ray filmography during pure aluminum welding, confirmed that porosity generation was attributed to bubble formation at the keyhole bottom due to unstable, dynamical gas conditions, excessive evaporation. A similar mechanism could apply for welding of steel. For the pulsed laser keyhole welding, different mechanisms are applied but it is also related to melt flow stability according to Zhou et al. [4]. It was identified by Zhou and Tsai [5] that porosity occurs when the solidification rate of the molten metal is higher than backfilling speed of liquid metal within solidification process time range. This mechanism possibly could apply for continuous wave laser case during unstable keyhole dynamics. Moreover, it was found that larger pores and their frequency occurred for higher depth-to-width ratio. However, a few studies were made concerning porosity in deep penetration welding of steel.

The solidification cracking problem is common for high depth-to-width-ratio welded joints. It is a very complex phenomenon and is still not completely understood. It might be related to the fact that it occurs within very short time during solidification and any kind of in-situ measurements are very challenging [6], especially in case of thick plates (>10-20 mm). However, numerous theories have been proposed over the years. Many of these are related to high stress/strain field which is more frequently found in the root zone [7-9] in deep penetration welds. It is well known that thermal stresses during welding causing large distortion due to plastic deformation caused by thermal expansion and subsequent shrinkage or contraction strains during cooling or final solidification stage [10]. This may, in turn, result in a complicated state of stress/strain in a hardened welding seam. Many researchers [11, 12] showed that the driving force of the solidification cracking is stress/strain evolution at the trail of the weld pool within the mushy zone containing solid and liquid fractions (region between solidus and liquidus points) which is defined by the ductility curve in brittle temperature range (BTR) during solidification shrinkage. Cracking can also be related to faster cooling rates causing harder microstructures with high strains during solid-state transformation (transformation strain), e.g. martensite which has a distorted lattice. However, no in-depth studies were performed for deep penetration welds and cannot be termed as solidification or hot cracking since it occurs during solid-state transformation. The effect of solidification behavior, the prior austenite grain growth direction, can also be a criterion for solidification cracking susceptibility. The dependency of the dendrite growth angle on solidification cracking susceptibility was clearly shown by Gollnow et al. [13] in case of different stainless steels. This can be also applicable in case of carbon steel concerning columnar prior austenite grain solidification mode. Another important factor is the chemical composition in specific areas (e.g. centerline in the laser part, i.e., root area) during solidification. If there is an excess of sulphur, due to a segregation behavior in a liquid film around dendrites/columnar grains, the probability of crack occurrence is significantly increasing according to Yu et al. [14] due to formation of low melting phases (e.g. FeS). Therefore, the selected welding consumable can also be an important factor. In the work performed by Gittos et al. [15], where a 25 kW CO_2 laser beam was used, different types of solidification cracking can be generated depending on steel chemical composition (C-Mn steels), weld geometry (controlled by changing focus spot) and grain morphology.

In this work, the experimental and analytical studies on deep welds in 45 mm thick plates and corresponding numerical simulation by finite element modelling (FEM) were performed to determine porosity and cracking formation. Non-destructive X-ray testing was used to recreate the morphology of the porosity and cracking in deep and narrow welds as well as their location and frequency.

2. Methodology

2.1. Equipment and materials

The experimental LAHW setup is shown in Fig. 2, with the geometrical setup parameters listed in Table 1. The laser was a 15 kW ytterbium fiber laser (IPG Laser GmbH, type YLR-15000 (fiber core diameter 400 μm, beam

parameter product 10.3 mm·mrad, wavelength 1070 nm). The laser was operated in the continuous wave mode, focused at the material surface by 300 mm focal length optics to a spot size of 800 µm diameter with Rayleigh length ±4 mm. The optical fiber of the laser was tilted at an angle of 7°30' from perpendicular to prevent back reflections damaging. Fronius TPS4000 VMT Remote GMAW power source was used with the torch in a 60° tilted position. The wire feeder is a combination of a continuous feeding unit VR7000 with a Robacta drive unit (Fronius GmbH) that carries out the back and forth motion of the wire tip which enables the CMT arc mode used in some of the experiments. The welding was carried out using an articulated robot from Motoman. The process was observed by high speed image (HSI) camera with a pulsed illumination 500 W (maximum 2% duty cycle) diode laser from Cavitar.

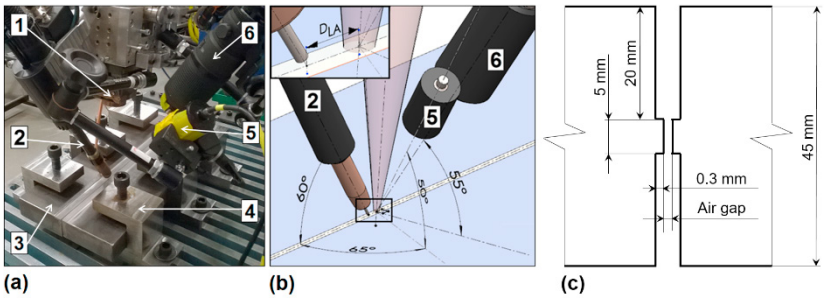

Fig. 1. Experimental setup (a, b): 1 – fiber laser beam welding head; 2 – GMAW torch; 3 – workpieces; 4 – fixturing equipment; 5 – illumination diode laser; and 6 – high speed imaging equipment. (c) Groove preparation.

Table 1. Constant geometrical and welding parameters.

Parameter	Value and dimension	Parameter	Value and dimension
Laser power	15 kW	Filler wire stick-out	15±1 mm
Focal point position	–7 mm	Process distance (D_{LA})	4±0.5 mm
Focal length	300 mm	Shielding gas composition	82% Ar + 18% CO_2
Focused spot diameter	800 µm	Shielding gas flow rate	25 l/min
Rayleigh length	±4 mm	Arc mode	Pulsed
GMAW torch angle	60±2°	Arc position	Trailing

A microalloyed (non-commercial) high strength steel was used. The plates of 500 mm × 120 mm × 45 mm were prepared and clamped with the fixture shown in Fig. 1. The edges were milled having low roughness. A 1.2 mm metal-cored filler wire (Kobelco TrustArc MX-A55T) was used. The chemical composition and mechanical properties of the base metal and filler wire are represented in Table 2 and Table 3 respectively.

Table 2. Chemical composition (wt.%) of the base plate and filler wire. (Balance is Fe).

Material	C	Si	Mn	P	S	V	Ni	Cr	Cu	Mo
Base metal*	0.036	0.082	1.97	0.007	0.001	0.01	0.7	0.07	0.18	0.1
Filler wire	0.06	0.35	1.41	0.011	0.017	0.01-0.05	1.48	0.02-0.15	0.04-0.30	0.01-0.20

*Al, Nb and Ti was present in very small amounts (< 0.03 wt.%)

Table 3. Mechanical properties of base plate and filler material.

Material	Yield strength, $R_{p0.2}$ (MPa)	Ultimate tensile strength, R_m (MPa)	Break elongation, A_5 (%)
Base material	522	629	23
Filler wire	518 (min. 460)	598 (min. 530)	31 (min. 20)

2.2. Process variables

The main variables were selected to achieve a stable process in filling larger gaps, including the welding speed, air

gap, and filler wire feed rate. The variable parameters are presented in Table 4. To achieve full penetration was not the main target here, but was possible with optimized parameters, as presented elsewhere [9]. The arc source parameters (voltage, frequency, current, background current and pulse time) were pre-set based on specific synergic lines which means that the filler wire feed rate (*WFR*) was controlled by pre-set arc current and voltage according to the manufacturer in order to provide a stable wire melting.

A double-sided welding technique was applied (one-pass from each side) due to the weld penetration limitations of the equipment. An I-straight shaped bevelling with a mid-plate 5 mm root face width was used as shown in Fig. 1c.

The total line energy input for LAHW (Q_H, kJ/mm) is calculated as a sum of the laser beam (Q_L, kJ/mm) and the arc energy input (Q_A, kJ/mm):

$$Q_H = Q_L + Q_A = \frac{60 \cdot P_L \cdot \eta_L}{1000 \cdot v_t} + \frac{60 \cdot P_A \cdot \eta_A}{1000 \cdot v_t} \quad (1)$$

where P_L is laser power (in kW), P_A is arc power (in kW: (current × voltage)/1000), v_t is travel speed (m/min), η_A is arc efficiency factor (0.8 for GMAW source), and η_L is laser beam efficiency factor (0.7 absorption coefficient for low alloy steel and 1 μm wavelength laser beam).

Table 4. Process variables.

Weld No.	Welding speed, m/min	Air gap, mm	*WFR*, m/min (current, A/voltage, V)	Arc heat input, kJ/mm	Laser heat input, kJ/mm	Total heat input, kJ/mm
1	0.6	0.4	7 (188/28.6)	0.43	1.05	1.48
2	0.8	0.3	9 (223/28.9)	0.38	0.79	1.17
3	0.8	0.8	10 (256/28.6)	0.44	0.79	1.23
4	0.95	0.8	13 (303/30.1)	0.46	0.67	1.13
5	1.2	1.0	18 (379/34.1)	0.52	0.53	1.05

2.3. Non-destructive and destructive testing

The welds were subjected to X-ray photography according to EN 1435 (ISO 17636-1 and -2). The specimens were cut longitudinally from each side with 10 mm distance from weld centreline and X-raying was applied from the side of the welded coupons. X-ray films were also taken from the top. Ultrasonic inspection was performed from the side according to EN ISO 17640. In addition, samples were cut longitudinally to reveal internal imperfection.

2.1. Finite element modelling

Thermomechanical analysis of the welding process was performed using the ABAQUS. A subroutine DFLUX has been used to introduce the moving heat sources. The keyhole was modelled by a conical volumetric heat source. The arc model was based on Goldak's double ellipsoidal volumetric heat source [16]. A detailed description of the model can be found in [17]. The mechanical properties of the steel were assumed temperature independent: Young's modulus 210 GPa, yield strength 550 MPa, expansion coefficient 1.1×10^{-4} mm, and Poisson's ratio = 0.31.

3. Results and discussion

3.1. Porosity

The weld defects are schematically shown in Fig. 2. The effect of process parameters on porosity is outlined in Fig. 3. An increase in porosity is related to various process parameters. The best correlation is with welding speed and arc power. Moderate correlation with air gap and laser heat input. Since all welds had high depth-to-width ratio, they exhibit high susceptibility to porosity. An increased welding speed seems to enhance porosity, which seems to be reasonable since the faster cooling will facilitate entrapment of pores. An increased air gap had similar effect as the

travel speed. This implies that bubbles (filler with metal vapour) due to melt flow cannot escape from the weld pool from beneath but flows upwards or straight to rear part of weld pool. The porosity is further reduced by an increase in laser heat input, while the opposite is apparently the case for the arc heat input. In latter case, higher *WFR* might disturbed keyhole dynamics. Pores were mainly located at 1/4 depth distance from the root.

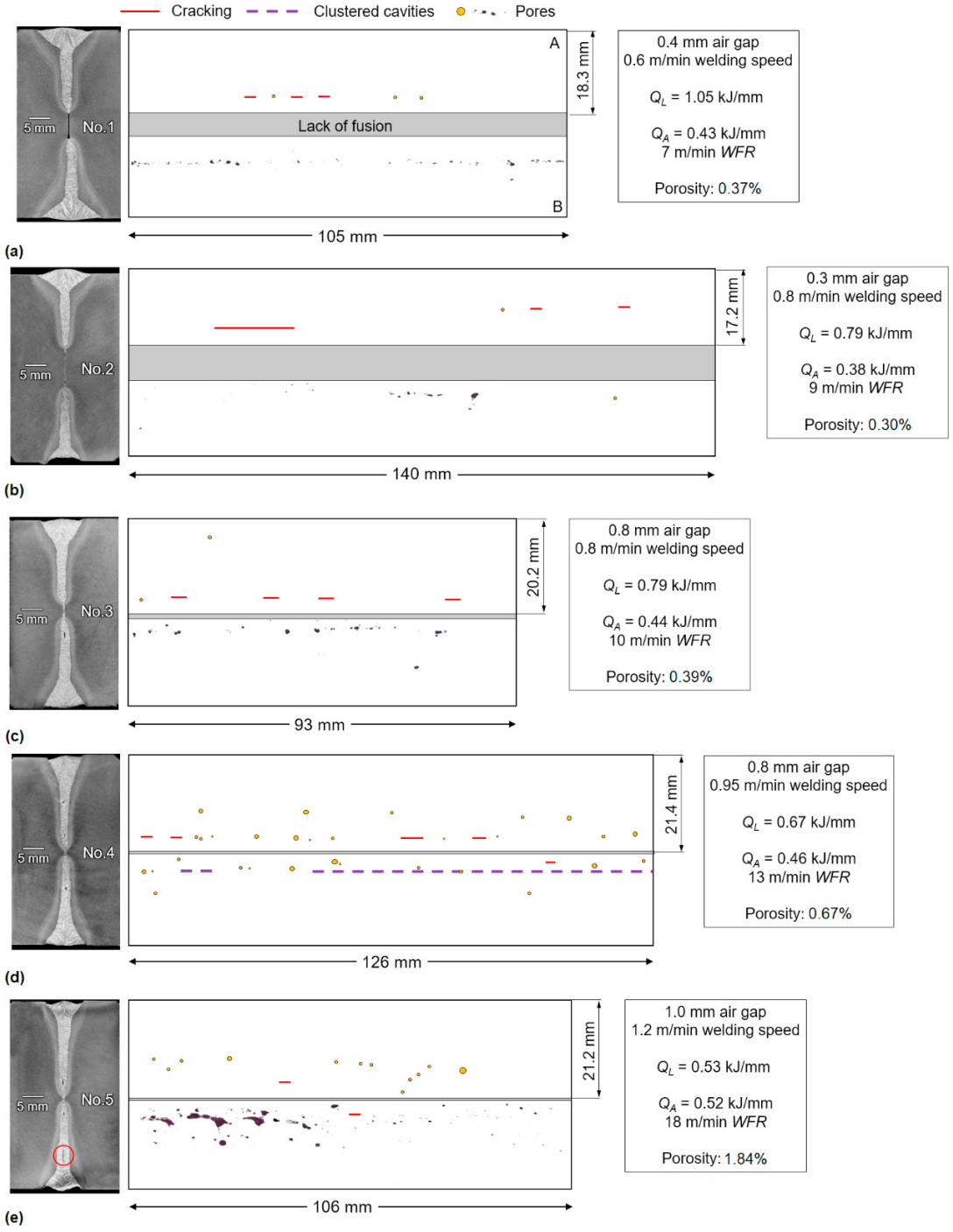

Fig. 2. Internal imperfections of welded joints (from side). Upper part (A) represents ultrasound with X-ray inspection and (B) is longitudinal cut.

Weld No. 4 had unstable processing in the root area generating much of clustered cavities which might indicate large cracks. This indicates very unstable condition and high possibilities of keyhole partial collapses.

According to Fig. 2, longitudinal mechanical cut (showed as bottom part of welds with B letter) showed much more porosity due to very high amount of small pores which cannot be spotted, or very difficult to spot, by ultrasound and X-ray testing. Therefore, destructive testing of deep and narrow welds are highly advisable over non-destructive testing according to the results.

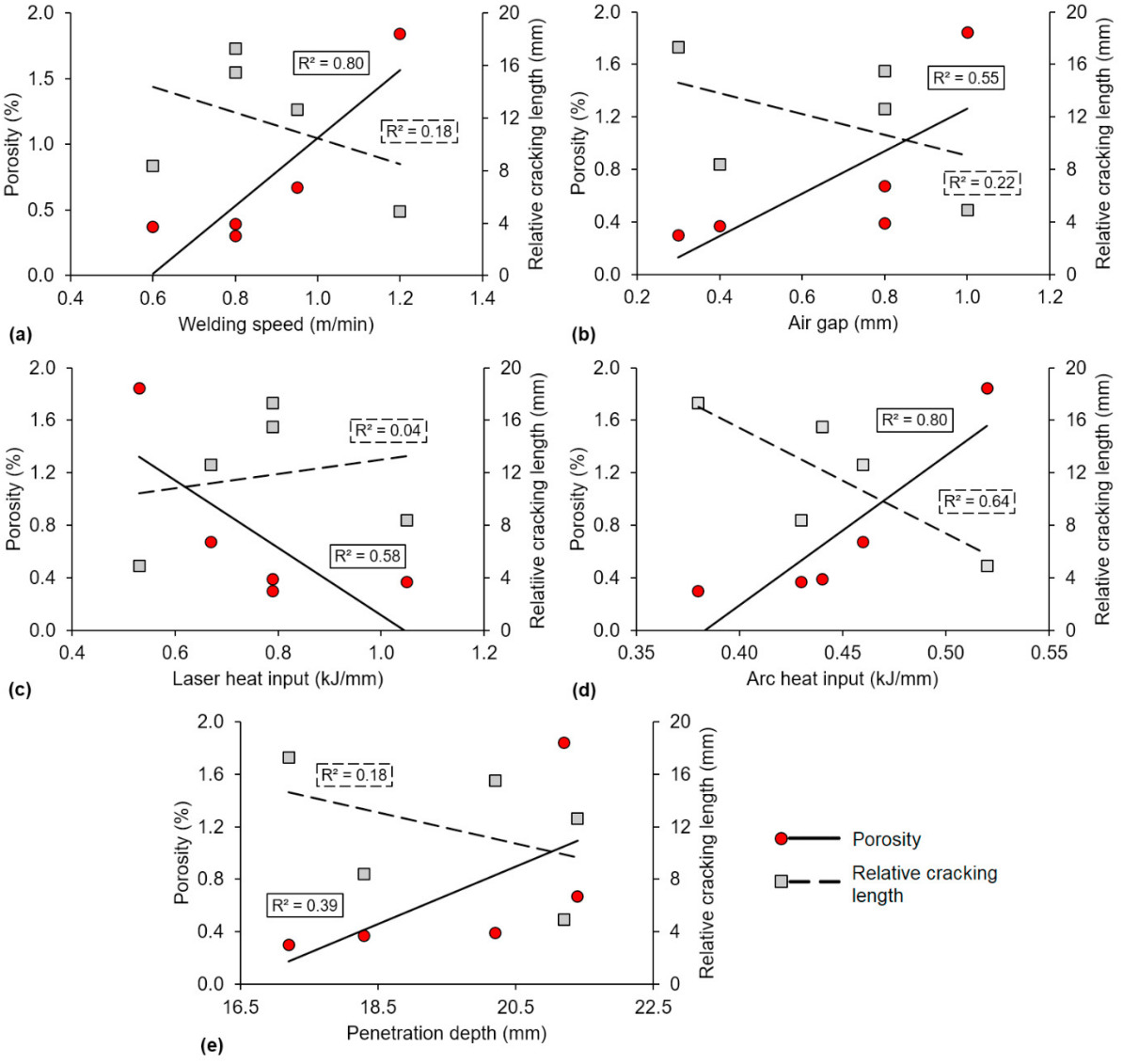

Fig. 3. Effect of process parameters on porosity and relative cracking length.

Accordingly, the keyhole dynamics was proposed and is schematically illustrated in Fig. 4, where the melt flow direction was proposed, based on both Frostevarg [18] and experimental observations within the present study. Two mechanisms for porosity formation can be identified: 1) pores from unstable keyhole dynamics in the bottom zone, Fig. 4a; 2) pores generated due to unstable keyhole rear wall dynamics, Fig. 4b. Both mechanisms can possibly be induced simultaneously.

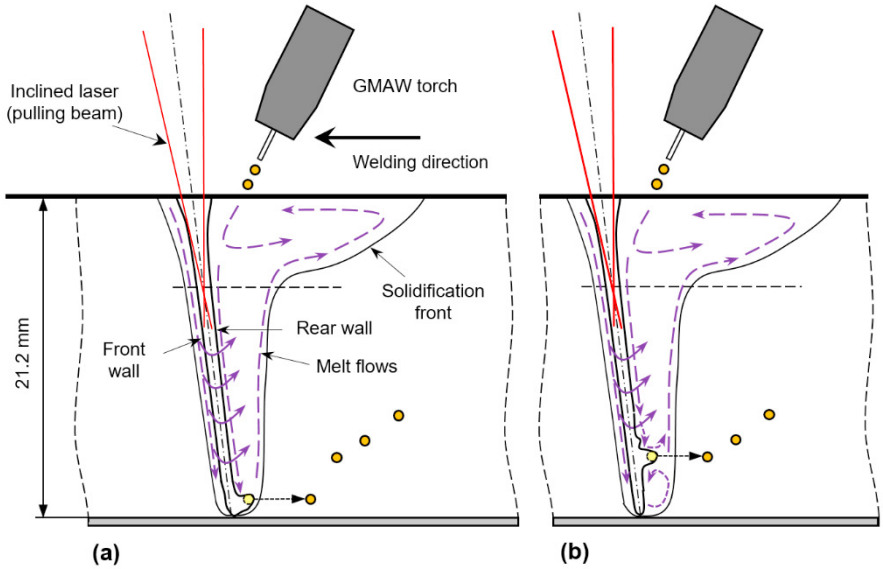

Fig. 4. Pore generation mechanisms.

Mechanism No. 1. The collapse of the keyhole can be induced by both unstable front and rear keyhole wall. The velocity of the molten metal at the front keyhole wall is very high during high power fiber laser processing [19-21]. There is an increased waviness at the bottom keyhole due to increased welding speed (see Fig. 3a), this will increase absorption with subsequent non-uniform vaporization, or excessive vapour metal at the bottom, forming the metal vapour filled pocket at the rear keyhole wall. Wang et al. [22] presented similar mechanism and the process was observed by application of the glass/steel sandwich technique (when keyhole is observed from the side through glassy material by high speed imaging) and X-ray filmography with tracing particles. Moreover, an applied larger gap caused keyhole opening area to be below the plate surface level, confirmed experimentally by HSI, which may in turn, cause unstable multiple reflections and unstable behaviour of the keyhole walls. The keyhole collapse cannot be confirmed, but consistent penetration depth was provided. However, it is shown experimentally and numerically by Zhang et al. [23] that prediction gave similar porosity generation mechanism with glass/steel sandwich technique. In addition, Otto et al. [24] numerically predicted that porosity formation in the lower zone is caused by keyhole collapse which was related to lower evaporation rating and pressure inside the keyhole with condensation phenomenon. Subsequently, after collapse, the pore was separated from the melt pool. Katayama [25] suggested that collapse at the keyhole root is caused by Rayleigh instability due to reduced power density.

Mechanism No. 2. The rear keyhole wall dynamic stability is dependent on vaporization phenomena during multiple trapped laser light reflections based on Fresnel absorption. Ai et al. [26] showed, by numerical simulation, that waviness of the rear keyhole wall is very high, resembling bulges. The same phenomenon was experimentally observed by Wu et al. [27] with application of the glass/steel sandwich technique with HSI. Due to a sudden excessive vaporization at the rear keyhole wall, higher pressure formed bulging into the molten pool. This in turn, can cause unstable melt flow and pores can be formed during solidification.

There are some porosity suppression mechanisms. For example, Matsumoto et al. [28] suggested that large spot diameter (with lower power intensity at the laser beam centre axis) and larger focus depth suppress porosity due to more stable keyhole dynamics, specifically at lower welding speeds. Tsukamoto et al. [13] proposed to use modulation of laser power by using squared-wave pulses including adjustments of base/peak power levels. However, the suppression mechanisms are only partly applicable for a certain case since they were performed within limited range of welding parameters and not studied in detail.

Welded joints were further assessed according to ISO 12932 [15] to identify quality level and suitability for production. In this case, an assumption is made that lack of fusion is not a defect. If lack of fusion is considered, all welds do not qualify to any level since maximum allowable lack of fusion for level D is 2 mm. Porosity density (in % of the total area) is characterized as function of the number of pores and their size (defect No. 2011 according to ISO

6520-1) and welds No. 1-3 qualifies to level B (since max. allowable density ≤ 1%), except for welds No. 4 and 5 which had more than 1.5% porosity and corresponds to level D.

3.2. Solidification cracking

3.2.1. Morphology and location of cracks

It has been found that solidification cracks are predominantly located in the root area. Their appearance tends to be 'longitudinal' parallel with the welding direction and located at weld centreline. No 'transversal' cracking was observed in any sample. This indicates that residual stresses are very high in this area locally exceeding yield strength of the material. The cracking appearance is not continuous but has intermittent behaviour. Very similar behaviour was reported by Wiklund et al. [7] and Quiroz et al. [29] who also showed that increased restraint intensity (clamping force) promotes a large number of cracks.

3.2.2. Effect of welding parameters

According to Fig. 3, solidification has low dependency on studied process parameters. A moderate correlation is only revealed with arc heat input, or *WFR*. However, it is unlikely that arc heat input can affect the cracking in the root area since supplied additional heat from the arc has very low effect on cooling rate in case of deep penetration welding of thick plate.

3.2.3. Effect of solidification characteristics

Columnar and equiaxed solidification modes are usually developed in welding of low carbon low alloy steels. Equiaxed solidification microstructure has much lower susceptibility for cracking than columnar microstructure. In the case of columnar grains, a bowing angle can be important. There is a possibility that small equiaxed prior austenite grains at the weld centreline may be effective for suppression crack formation and its propagation when the transient thermal tensile stress exceeds the actual yield strength in weld metal. All welds had very similar morphology of prior austenite grain with specific direction which is horizontally parallel to weld centreline. As a conclusion, the relation of solidification cracking within selected range of process parameters, the welds fall to a high crack sensibility range.

Weld No. 3 was used for numerical simulation. The numerical results show good agreement with experimental observations. This is shown in Fig. 5a, including the susceptible area for solidification cracking (area 'a' in Fig. 5a). The temperature range of the mushy zone is set as 1420-1520 °C, represented by the yellow zone defined in Fig. 5b. In the upper area of the weld, the cooling rate of the mushy zone is 370 °C/s (or $\Delta t_{15/14} = 0.27$ s), while it is 3125 °C/s (or $\Delta t_{15/14} = 0.032$ s) in the root area. Such extremely fast cooling rates indicate that there is high local stress/strain fields. Therefore, the liquid films between columnar grains impair the weld metal resulting in low resistance to cracking. The cooling rates of the mushy zone may be used as a criterion to predict solidification cracking for future application using transient heat transfer models as well as to determine the columnar-to-equiaxed transition solidification mode. Since welds have similar penetration depth and fusion zone width, they fall into the same category due to very similar cooling rates and exhibit columnar solidification mode. Possibly, the range of chosen process parameters is too narrow to identify conditions for crack-free welds. It is therefore summarized that narrow and deep welds, corresponding to > 15 mm penetration depth and 2-3 mm width of fusion zone, is very likely to have solidification cracking.

Based on these results, it is reasonable to suggest to reduce the welding speed (increase the heat input) to provide more equiaxed solidification at the weld centreline. Here, the use of larger laser spot diameter might be a good alternative. Better distribution of welding wire to the root area in deep welds may also mitigate the cracking problem. Another proposal is to apply preheating.

3.2.4. Effect of solidification on stress distribution

According to the simulation results, high stresses were accumulated close to the root area acting as a main driving force for the cracking as shown in Fig. 6a. Normal transverse stress shows low stress values (see Fig. 6b). Two normal stress components were the most significant; longitudinal stress (along y-axis) and through-thickness stress (along z-axis) for Fig. 6c and Fig. 6d respectively. Shear stresses were negligible. Stresses in the upper zone (closer to the upper surface, in the middle) are also high but due to high amount of filler wire which provides some acicular ferrite

and wider zone with slower cooling rates, cracks has low probability to occur. While high stresses exceeding yield strength at the deeper areas were developed, within temperature range of the mushy zone, with high amount of hard microstructures (confirmed by the previous results [30]). Therefore, the occurrence of cracking is very high.

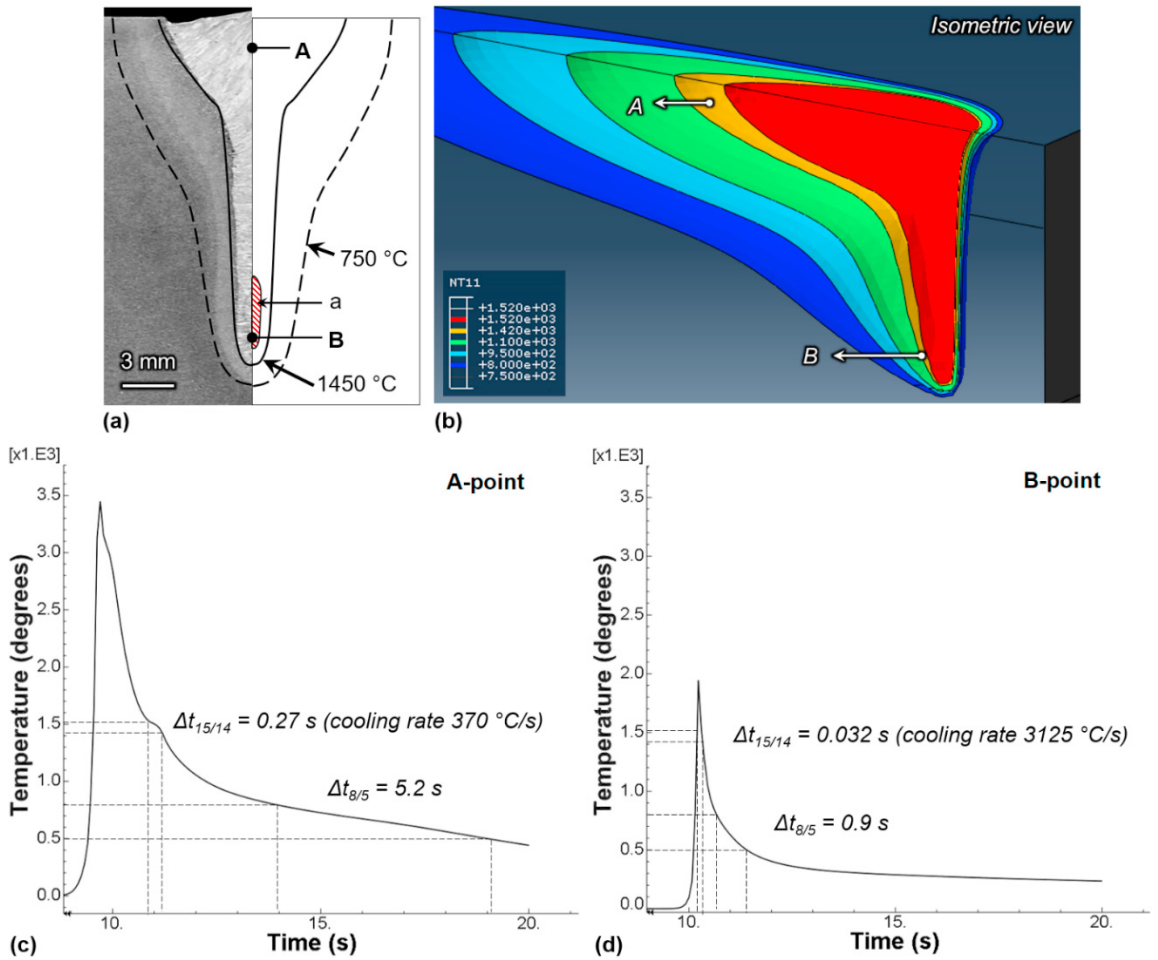

Fig. 5. (a) Comparison of weld bead profile between simulation and experimental measurement (weld No. 3) and (b) different thermal zones during welding process. Estimation of cooling rates based on thermal history by FEM at (c) A-point and (d) B-point.

4. Conclusions

From the analysis of the experimental results and simulations, the following can be concluded:

- Laser-arc hybrid welding is very susceptible for porosity and solidification cracking formation in deep penetration welding mainly attributed to very high depth-to-width ratio
- The porosity level increases with increasing welding speed and air gap between the plates in deep penetration welding
- Two mechanism of porosity formation is proposed, related to stability of the keyhole walls
- Solidification cracking was mainly located in the root at the weld centreline where columnar grain morphology was developed having low resistance for crack growth. Alternative solution to avoid cracking is to apply lower welding speed (higher heat input) by increase spot diameter

- Numerically estimated cooling rates in the mushy zone in the root area are faster compared to crack-free upper area of the welds
- Numerically estimated stress and strain fields show good agreement with experimental observations of the cracking occurrence with their highest values in the root of deep penetration welds

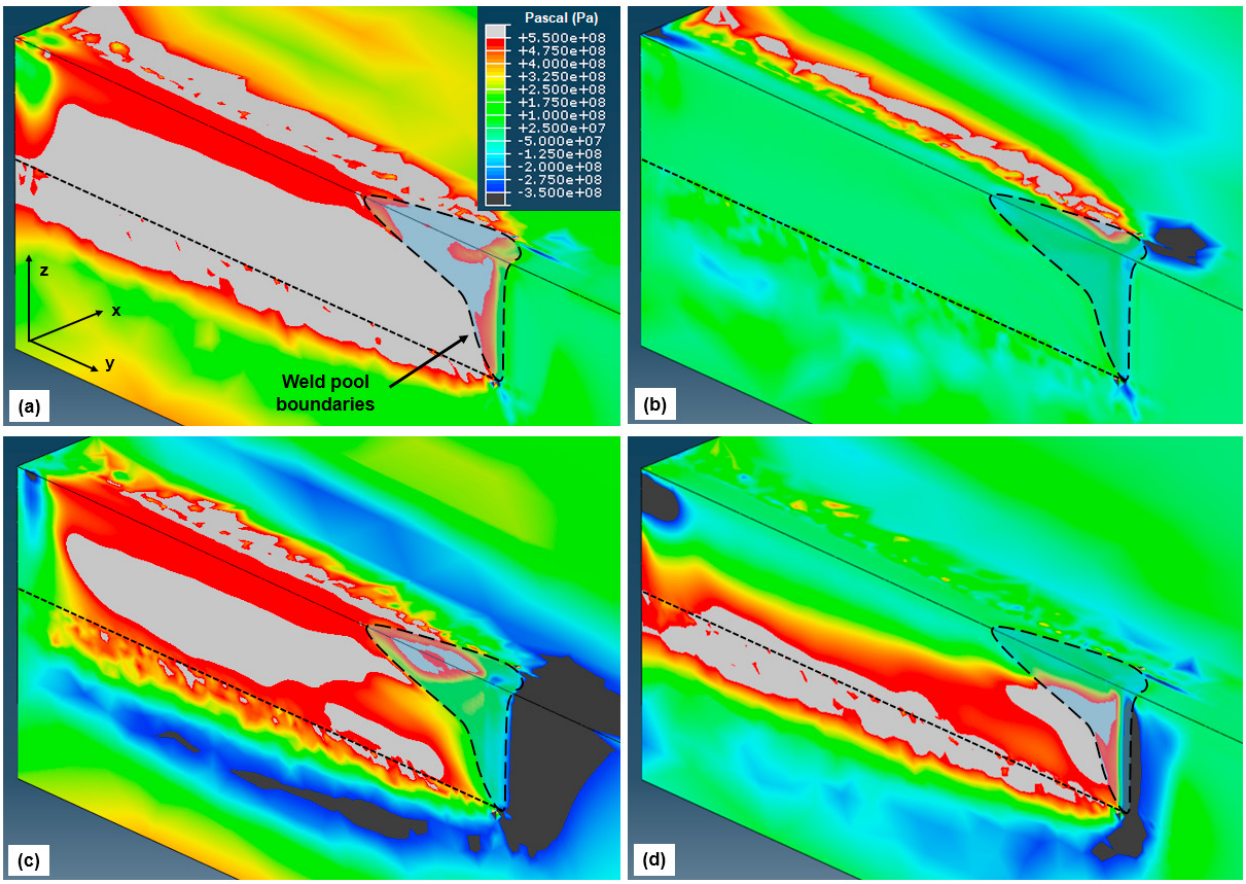

Fig. 6. 3D stress field during deep penetration welding (Weld No. 3) where (a) maximum principal stress, (b) transverse stress, (c) longitudinal stress, and (d) through-thickness stress.

Acknowledgements

The authors wish to thank the Research Council of Norway for funding through the Petromaks 2 Programme, Contract No. 228513/E30. The authors acknowledge funding from the EC Research Fund for Coal and Steel, RFCS, project OptoSteel, no. 709954. The financial support from ENI, Statoil, Lundin, Total, JFE Steel Corporation, Posco, Kobe Steel, SSAB, Bredero Shaw, Borealis, Trelleborg, Nexans, Aker Solutions, FMC Kongsberg Subsea, Marine Aluminium, Hydro and Sapa are also acknowledged. Vitec AS is appreciated for carrying out the ultrasonic and X-ray radiographic testing.

References

[1] ISO 17639 - Destructive tests on welds in metallic materials - Macroscopic and microscopic examination of welds, (2003) 9.
[2] S. Katayama, Y. Naito, S. Uchiumi, S. Mizutani, Physical Phenomena and Porosity Prevention Mechanism in Laser-Arc Hybrid Welding, Transactions of JWRI, 35 (2006) 13-18.

[3] ISO 22826 - Destructive tests on welds in metallic materials - Hardness testing of narrow joints welded by laser and electron beam (Vickers and Knoop hardness tests), (2005) 16.
[4] J. Zhou, H.-L. Tsai, P.-C. Wang, Transport Phenomena and Keyhole Dynamics during Pulsed Laser Welding, Journal of Heat Transfer, 128 (2006) 680-690.
[5] J. Zhou, H.-L. Tsai, Porosity Formation and Prevention in Pulsed Laser Welding, Journal of Heat Transfer, 129 (2006) 1014-1024.
[6] N. Bakir, A. Gumenyuk, M. Rethmeier, Investigation of solidification cracking susceptibility during laser beam welding using an in-situ observation technique, Science and Technology of Welding and Joining, 23 (2018) 234-240.
[7] G. Wiklund, O.M. Akselsen, A.J. Sørgjerd, A. Kaplan, Geometrical aspects of hot cracks in laser-arc hybrid welding, Journal of Laser Application, 26 (2014).
[8] M.O. Gebhardt, A. Gumenyuk, M. Rethmeier, Solidification cracking in laser GMA hybrid welding of thick-walled parts, Science and Technology of Welding and Joining, 19 (2013) 209-213.
[9] I. Bunaziv, J. Frostevarg, O.M. Akselsen, A.F.H. Kaplan, The penetration efficiency of thick plate laser-arc hybrid welding, Int J Adv Manuf Technol, 97 (2018) 2907-2919.
[10] N. Bailey, S.B. Jones, The Solidification Cracking of Ferritic Steel During Submerged Arc Welding, Welding Journal, 57 (1978) 217-231.
[11] ISO 13919-1 - Welding - Electron and laser-beam welded joints - Guidance on quality levels for imperfections - Part 1: Steel, (1996) 7.
[12] G. Agarwal, A. Kumar, H. Gao, M. Amirthalingam, S.C. Moon, R.J. Dippenaar, I.M. Richardson, M.J.M. Hermans, Study of Solidification Cracking in a Transformation-Induced Plasticity-Aided Steel, Metallurgical and Materials Transactions A, 49 (2018) 1015-1020.
[13] S. Tsukamoto, I. Kawaguchi, G. Arakane, H. Honda, Keyhole behaviour in high power laser welding, Proc. SPIE, 1st Intl. Symp. on High Power Laser Macroprocessing, 4831 (2002) 251-256.
[14] Y. Erjing, Y. Huiyun, L. Quan, S. Zhongyao, Sulphur-induced ductility-dip cracking in low carbon steel weld metal, Welding International, 1 (1987) 686-690.
[15] ISO 12932 - Welding - Laser-arc hybrid welding of steels, nickel and nickel alloys - Quality levels for imperfections, (2013) 25.
[16] J. Goldak, M. Akhlaghi, Computational Welding Mechanics, Springer, 2005.
[17] I. Bunaziv, O.M. Akselsen, J. Frostevarg, A.F.H. Kaplan, Laser-arc hybrid welding of thick HSLA steel, Journal of Materials Processing Technology, 259 (2018) 75-87.
[18] J. Frostevarg, Factors affecting weld root morphology in laser keyhole welding, Optics and Lasers in Engineering, 101 (2018) 89-98.
[19] J. Pocorni, D. Petring, J. Powell, E. Deichsel, A.F.H. Kaplan, Measuring the Melt Flow on the Laser Cut Front, Physics Procedia, 78 (2015) 99-109.
[20] I. Eriksson, J. Powell, A.F.H. Kaplan, Melt behavior on the keyhole front during high speed laser welding, Optics and Lasers in Engineering, 51 (2013) 735-740.
[21] I. Eriksson, J. Powell, A.F.H. Kaplan, Measurements of fluid flow on keyhole front during laser welding, Science and Technology of Welding and Joining, 16 (2011) 636-641.
[22] H. Wang, M. Nakanishi, Y. Kawahito, Dynamic balance of heat and mass in high power density laser welding, Optics Express, 26 (2018) 6392-6399.
[23] D. Zhang, M. Wang, C. Shu, Y. Zhang, D. Wu, Y. Ye, Dynamic keyhole behavior and keyhole instability in high power fiber laser welding of stainless steel, Optics & Laser Technology, 114 (2019) 1-9.
[24] A. Otto, R.G. Vázquez, U. Hartel, S. Mosbah, Numerical analysis of process dynamics in laser welding of Al and Cu, Procedia CIRP, 74 (2018) 691-695.
[25] S. Katayama, Handbook of Laser Welding Technologies Woodhead Publishing 2013.
[26] Y. Ai, P. Jiang, C. Wang, G. Mi, S. Geng, Experimental and numerical analysis of molten pool and keyhole profile during high-power deep-penetration laser welding, International Journal of Heat and Mass Transfer, 126 (2018) 779-789.
[27] D. Wu, X. Hua, L. Huang, F. Li, Y. Cai, Observation of the keyhole behavior, spatter, and keyhole-induced bubble formation in laser welding of a steel/glass sandwich, Welding in the World, (2019).
[28] N. Matsumoto, Y. Kawahito, K. Nishimotoa, S. Katayama, Effects of laser focusing properties on weldability in high-power fiber laser welding of thick high-strength steel plate, Journal of Laser Applications, 29 (2017) 012003.
[29] V. Quiroz, M. Gebhardt, S. Gook, A. Gumenyuk, M. Rethmeier, Hot cracking in high power laser beam welding of thick high strength structural steels under restraint conditions, Proceedings of the 29th International Congress on Applications of Lasers and Electro-Optics (ICALEO), (2010) 225-232.
[30] I. Bunaziv, O.M. Akselsen, J. Frostevarg, A.F.H. Kaplan, Deep penetration fiber laser-arc hybrid welding of thick HSLA steel, Journal of Materials Processing Technology, 256 (2018) 216-228.